Journal of Coastal Research	18	1	25–38	West Palm Beach, Florida	Winter 2002

Modulation of Surf Zone Processes on a Barred Beach Due to Changing Water Levels; Skallingen, Denmark

Troels Aagaard

Institute of Geography
University of Copenhagen
Oster Voldgade 10
DK-1350 Copenhagen K., Denmark
E-mail: taa@geogr.ku.dk

ABSTRACT

AAGAARD, T., 2002. Modulation of Surf Zone Processes on a Barred Beach Due to Changing Water Levels; Skalligen, Denmark. *Journal of Coastal Research,* 18(1), 25–38. West Palm Beach (Florida), ISSN 0749-0208.

Three field experiments on surf zone morphodynamics were conducted on a beach along the exposed Danish North Sea coast. This beach is microtidal (spring tidal range approximately 1.7 m) but it is characterized by a relatively large ratio between spring tidal range and nearshore gradient (TR/β). Surf zone processes were modulated due to water level changes occurring at tidal and storm surge frequencies. Using cross-shore arrays of electromagnetic current meters, pressure sensors and optical backscatter sensors, it was found that offshore and surf zone wave heights increased with increasing water levels, while for selected instrument positions, cross-shore mean current speeds increased at high tide in the intertidal zone and at low tide in the subtidal zone. When subtidal bars were linear and shore-parallel, mean cross-shore currents were directed offshore; in the case of three-dimensional bars featuring shoals and rip currents, mean currents were directed onshore across bars and offshore in rip channels with maximum current speeds at low tide. In consequence, net sediment transport patterns were modulated on a tidal time scale. At times of high water levels, sediment transport tended to be directed onshore in the subtidal zone and offshore in the intertidal zone with the reverse occurring when water levels were relatively low. Conceptually, this should lead to less accentuated bar topography in comparison to tideless beaches and such modulations are probably a major reason for the low-relief and comparatively stable bar features generally found on beaches subjected to tides. Finally, it is speculated that on longer time scales, systematic changes in water level may result in systematic and predictable profile responses.

ADDITIONAL INDEX WORDS: *Waves, currents, tides, storm surges, sediment transport, morphodynamics.*

INTRODUCTION

Most beaches are to a greater or lesser extent subjected to water level fluctuations due to tides, storm surges, or phenomena occurring on longer (*e.g.* annual) time scales. The morphology exhibited by micro-, meso- and macrotidal beaches, respectively, has been discussed by WRIGHT *et al.* (1982), SHORT (1991) and MASSELINK (1993), amongst others. These observations indicate that as the tidal range increases, the gradient of the nearshore tends to become more shallow and the morphology becomes increasingly subdued and less mobile (see also DAVIS *et al.,* 1972; JAGO and HARDISTY, 1984 and WRIGHT *et al.,* 1987). It is generally thought that the reason for topographic smoothing is that the shoaling wave, surf and swash zones are displaced laterally across the profile through the tidal cycle, but no quantitative explanations of how exactly this would influence sediment transport processes at a given point were offered. Studies of profile variability due to water level changes on annual time scales were reported by *e.g.* HANDS (1977) who observed a landward migration of nearshore bars as well as beach erosion caused by rising lake levels in Lake Michigan.

99061 received 18 August 1999; accepted in revision 16 September 2000.

On the other hand, field studies on the modulation of hydrodynamic and sediment transport processes as affected by water level changes, *i.e.* the physical processes causing profile change have been rare, particularly with regard to the effects such modulations and their magnitude might have on the morphology. On a microtidal beach, THORNTON and KIM (1993) and FEDDERSEN *et al.* (1997) demonstrated that during low-tide, high-energy conditions, longshore currents were maximum over the bar due to strong dissipation of incident wave energy. At high tide, less incident wave energy was dissipated over the bar and the longshore current became weaker with a maximum located over the landward bar slope/outer trough region. Hence, while the tidally-induced water level changes did shift the longshore current maximum across the profile, the interaction between the topography and the hydrodynamics resulted in weaker overall currents at high tide.

Consistent with such an increased dissipation of incident wave energy at low tide over nearshore bars, rip current circulation also appears to intensify at low tide (SONU, 1972; BRANDER, 1999). The effects of increasing/decreasing incident wave dissipation upon low-frequency (infragravity) energy is not clear. DAVIDSON *et al.* (1993) reported that velocity variance at infragravity frequencies was more significant at low tide, while THORNTON *et al.* (1996) argued that long waves are not expected to exhibit strong tidal signature as they depend

mainly on offshore incident wave heights (GUZA and THORNTON, 1982).

These studies have increased our understanding of hydrodynamic changes in the surf zone as a result of shifting water levels but little is known about the link between hydrodynamics and morphology, *i.e.* the sediment transport and how this transport may be affected by the hydrodynamic modulations, for example those occurring over a tidal cycle. The present paper is an attempt to synthesize the results of a series of field experiments on a barred beach. The objective of these experiments was to study suspended sediment transport and morphodynamic linkages in a variety of morphological settings on a gently sloping dissipative beach subjected to tides and storm surges. The aim of this paper is to demonstrate: i) the modulation of surf zone hydrodynamics due to water level fluctuations, and ii) the ensuing effects upon suspended sediment transport. Finally, the implications of these findings relative to the nearshore morphology, particularly bar shape and overall profile change will be discussed. It is hypothesized that in the surf zone of gently sloping barred beaches, the periodic rise and fall of the mean water level will modulate the magnitude of mean flows and sediment transport patterns across bars on a tidal time scale, leading to a smoothing of the bar topography.

THEORY

Cross-shore and longshore sediment transport depend primarily upon incident wave height and the associated bed shear stresses, orbital asymmetries and the velocity of wave-generated mean currents. The cross-shore distribution of wave heights, outside as well as inside the surf zone, is given by the energy balance

$$\frac{\partial EC_g}{\partial x} = \langle \epsilon_b \rangle \tag{1}$$

(BATTJES and JANSSEN, 1978), where C_g is wave group velocity, $\langle \epsilon_b \rangle$ is wave energy dissipation and E is wave energy. Assuming that wave heights locally are Rayleigh-distributed, E is given by

$$E = 1/8 \rho g H_{rms}^2 \tag{2}$$

where ρ is sea water density, g is gravitational acceleration and H_{rms} is root-mean-square wave height. Outside the surf zone, dissipation is mainly due to bed friction (NIELSEN, 1984) and wave heights at breaking will be larger when the shoreface is narrow and steeply sloping than across wide, gently sloping shorefaces (WRIGHT, 1976). Further, assuming constant deep-water wave conditions, smaller water depths at low tide are expected to result in relatively smaller breaking wave heights compared to high tide conditions as frictional dissipation increases with decreasing water depths (BRETSCHNEIDER and REID, 1954).

Inside the breakpoint, $\langle \epsilon_b \rangle$ results primarily from incident wave breaking and in the case of a fully saturated surf zone (the inner surf zone), wave heights have been observed to be related to water depth, h, by

$$H_{rms} = \gamma h \tag{3}$$

where γ is a constant on the order of 0.3–0.45 (THORNTON and GUZA, 1982; SALLENGER and HOLMAN, 1985). SALLENGER and HOLMAN (1985) suggested $\gamma = 0.3 + 3.2 \tan\beta$, where β is nearshore slope. For a given point in the inner surf zone, *e.g.* on a bar crest, local wave height is therefore expected to decrease at low tide and increase at high tide. In the outer surf zone, breaking waves are not saturated and wave heights are not expected to be strongly dependent upon water depth. RUESSINK *et al.* (1998) found that incident waves started to break when $H_s/h \sim 0.33$ ($H_{rms}/h \sim 0.23$). Thus, the magnitude of γ may be viewed as a measure of the intensity of local wave energy dissipation due to breaking.

Field observations have indicated that incident wave asymmetries tend to increase towards a maximum at the breakpoint while they decrease landward of the breaking region (DOERING and BOWEN, 1985; THORNTON and GUZA, 1989a; RUSSELL and HUNTLEY, 1999). For a given point inside the wave breakpoint, *e.g.* a bar crest, wave asymmetry is therefore expected to be large at high tide and small at low tide. As incident wave asymmetries are usually directed onshore, this implies that the potential for onshore directed sediment transport should increase at high tide and decrease at low tide.

Wave-induced surf zone currents are driven by radiation stress gradients and fed by lagrangian Stokes drift and bore-induced mass transport (*e.g.* DALLY and OSIECKI, 1995). The cross-shore flux of longshore directed momentum, S_{yx} is balanced by the longshore directed bed shear stress, τ_b

$$\frac{\partial S_{yx}}{\partial x} = -\tau_{b,y} = -\rho c_f u_m V \tag{4}$$

where the bed shear stress has been linearized assuming that the longshore current velocity, V, is weak relative to the maximum wave orbital velocity, u_m (LONGUET-HIGGINS, 1970; THORNTON and GUZA, 1989b), ρ is the density of sea water and c_f is a friction coefficient. In shallow water, this component of the radiation stress is given by

$$S_{yx} = 1/8 \rho g H_{rms}^2 \sin\alpha\cos\alpha \tag{5}$$

(BOWEN, 1969) where α is angle of wave incidence. Analogously, for alongshore homogeneous flows the cross-shore flux of onshore directed momentum may be written

$$\frac{\partial S_{xx}}{\partial x} = -\rho g h \frac{\partial \bar{\eta}}{\partial x} - \tau_b = -\rho g h \frac{\partial \bar{\eta}}{\partial x} - \rho c_f u_m U \tag{6}$$

where U is the mean cross-shore current velocity and $\bar{\eta}$ is the set-up. Here, the cross-shore radiation stress gradient is balanced by a set-up and the cross-shore directed bed shear stress generated by the mean current, in this case the undertow. In shallow water, S_{xx} is given by

$$S_{xx} = 3/16 \rho g H_{rms}^2 \tag{7}$$

(LONGUET-HIGGINS and STEWART, 1964). Hence, mean current velocities are expected to depend on cross-shore wave energy gradients. How such gradients respond to changes in mean water level during a tidal cycle very much depends on topography. For a planar sloping beach, wave energy gradients and hence mean current distributions are expected to be similar in shape but displaced laterally across the profile over the

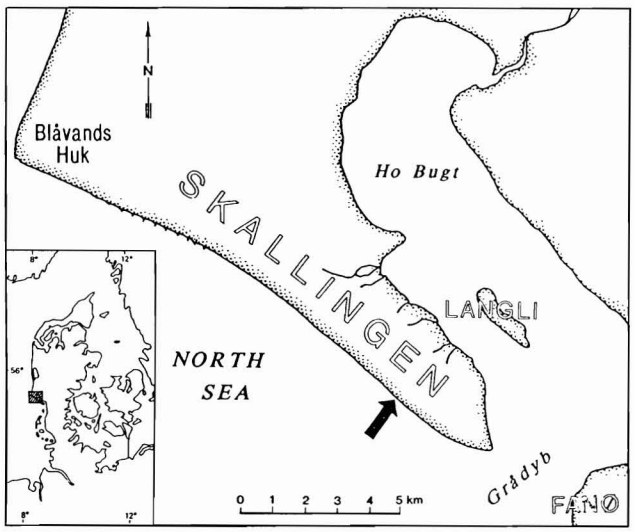

Figure 1. Map of the Skallingen spit and its surroundings. The experimental site is marked by an arrow.

course of a tidal cycle. In the case of a barred beach, it is possible that large wave energy gradients and wave height saturation only occur at low tide while waves are more weakly breaking across bars at high tide. This would result in increased longshore and cross-shore currents at low tide with increasing longshore and cross-shore sediment transport. Furthermore, when incident waves are saturated, (negative) wave energy gradients are expected to depend upon local bed gradients.

FIELD SITE AND EXPERIMENTS

The present field experiments were conducted at Skallingen which is a barrier spit facing the North Sea (Figure 1). This is a sandy uninterrupted shoreline and there are no engineering works within a distance of several kilometres of the field site. The subtidal zone is gently sloping ($\beta \approx 0.008$) while the intertidal zone slopes at $\beta \approx 0.025$. The tide is semi-diurnal with a spring tidal range around 1.7 m and the beach is hence classified as microtidal, although the gentle slope (horizontal shoreline excursion at spring tide; $TR/\beta \approx 70$ m) and the fact that the site is frequently subjected to storm surges enhance the effects of water level fluctuations. Moderate storms typically result in surges of approximately 0.5 m, while severe storms may elevate astronomically predicted tide levels by up to 3 m. Mean annual offshore wave heights are on the order of 0.5 m with wave periods of 4–6 seconds. During storms, the offshore wave height may increase up to 4 m with peak spectral wave periods of 10–13 seconds.

The mean grain size in the surf zone is 150–200μm and the nearshore profile comprises 2–3 subtidal (nearshore) bars as well as a highly mobile intertidal (swash) bar (Figure 2). The intertidal and inner subtidal bars are often dissected by rip channels.

The three field experiments were conducted during the fall

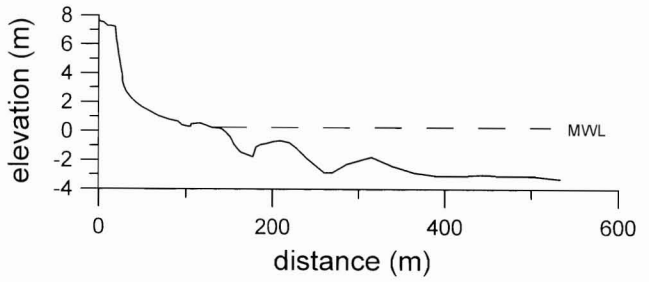

Figure 2. The cross-shore profile at the experimental site, surveyed on November 8, 1996.

seasons of 1994, 1995 and 1996 and were entitled SK94, SK95 and SK96, respectively. Figures 3 and 4 illustrate the typical morphology at the site during these three experiments. During SK94, instrument stations S1-S4 were located

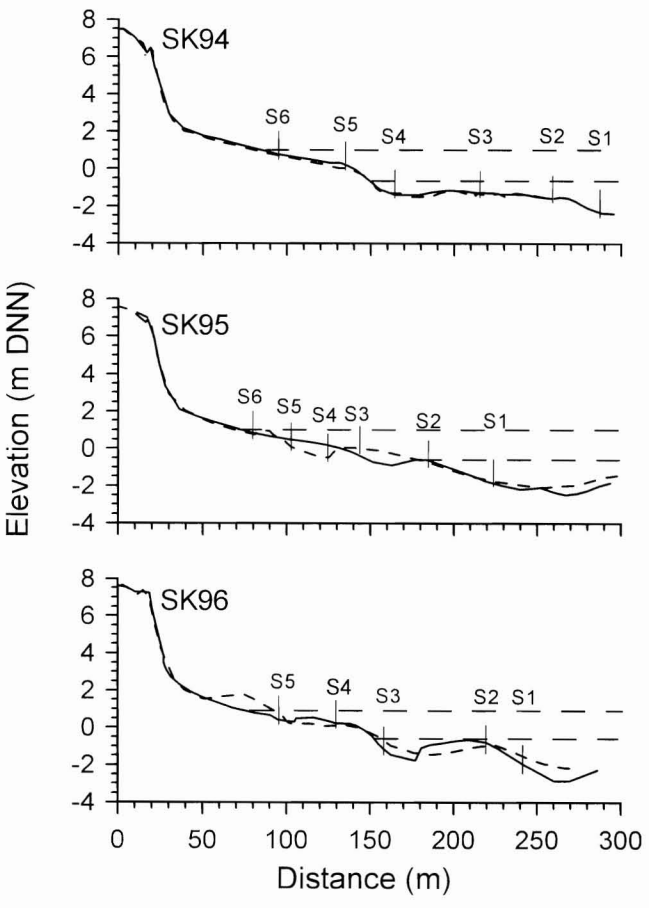

Figure 3. Cross-shore profiles across the beach/inner nearshore at the experimental site, surveyed on a) October 3 (dashed line) and 16 (solid line), 1994, b) October 12 (dashed line) and 29 (solid line), 1995 and c) October 22 (dashed line) and November 8 (solid line), 1996, respectively. The locations of the instrument stations S1–S6 are indicated for each experiment. Mean high and low tide levels are indicated by the horizontal dashed lines.

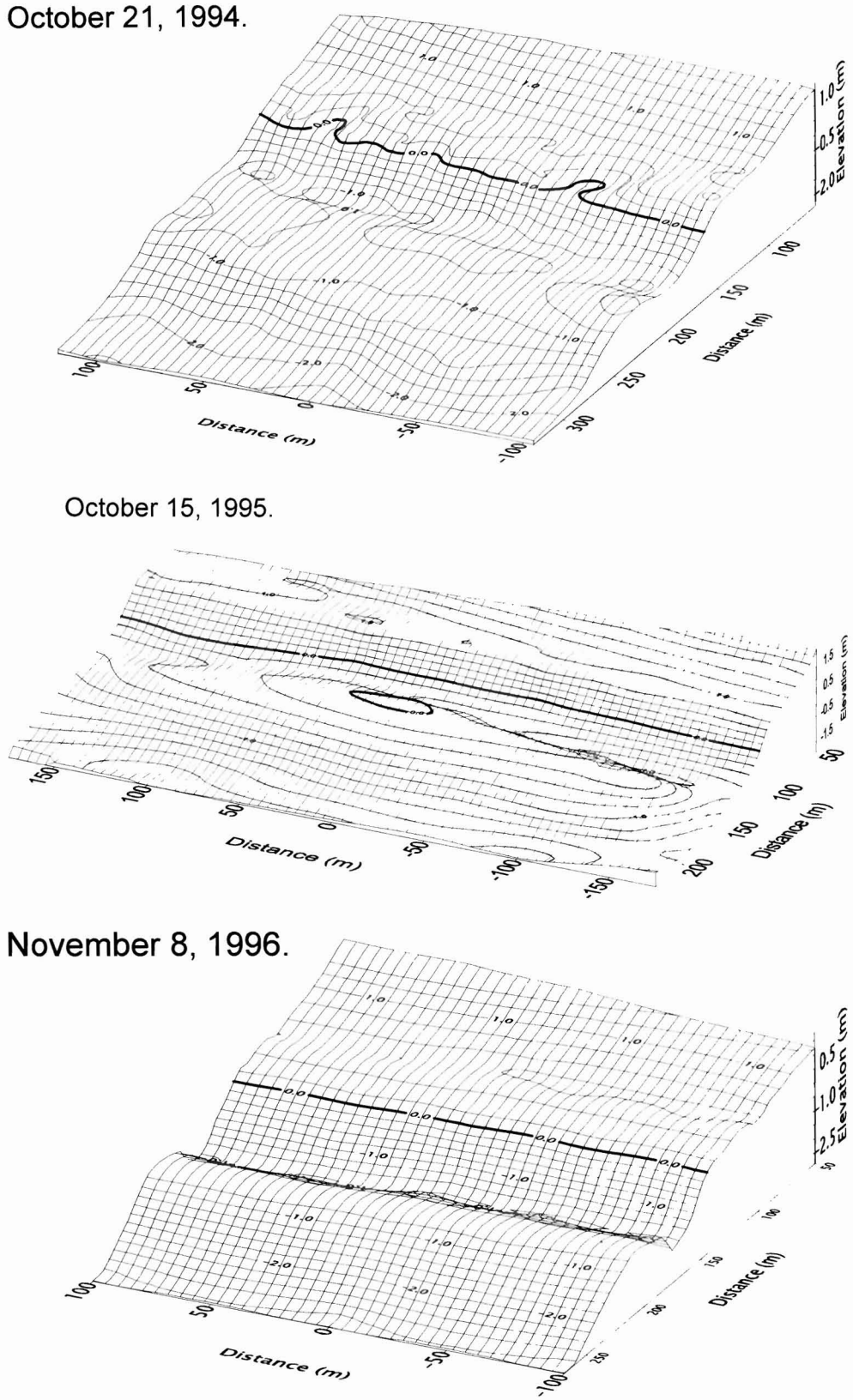

Figure 4. Plan view of the field site based on surveys and visual observations. a) 1994, b) 1995 and c) 1996. The instrument transects were at y = 0 m. Depth contours are in meters relative to DNN.

Table 1. *Aspect ratios of inner subtidal bar, spring tidal range (STR) and nearshore gradient for SK94-KS96 as well as a range of beaches described in the literature. Sources:* [1] Aagaard and Greenwood (1995), [2] Lee et al. (1998), [3] Wolf (1997), [4] Brander (1996), [5] Aagaard and Greenwood (1994), [6] Aagaard et al. (1994), [7] Ruessink et al. (1998).

Locality	Aspect Ratio		STR, m	β	STR/β
SK94	.0078	.0075			
SK95	.0085	.0088	1.8	.008	225
SK96	.0095	.018			
Burley Beach[1]	.018		~0	.009	~0
Duck[2]	.016		1.2	.011	109
Egmond[3]	.012		2.1	.009	233
Palm B.[4]	.020		1.6	.033	48
Stanhope B.[5]	.018		1.0	.009	111
Staengehus[6]	.021		0.3	.016	19
Terschelling[7]	.008		2.5	.005	500

in a rip channel crossing the inner subtidal bar (Figure 4). Low to moderate energy conditions prevailed throughout the experiment with maximum offshore significant wave heights of 1.40 m with wave periods around 8 seconds. Two minor surges occurred, each resulting in a superelevation of the mean water surface of 0.4–0.5 m. The bar topography remained stable during the 3½-week experimental period and only minor erosion and smoothing of the rip channel cross-section occurred (Figure 3).

The SK95-experiment again spanned the intertidal swash bar as well as the inner subtidal bar which had migrated into the lower intertidal zone at the beginning of the experiment. On this occasion, the main cross-shore transect was situated across the subtidal bar well away from rip channels which were located approximately 180 m either side of the transect (Figure 4). Hydrodynamics and sediment transport were monitored under a range of offshore wave energy conditions rather similar to SK94 (maximum significant offshore wave heights = 1.86 m with peak periods of 8 seconds) but in a different topographic setting. One minor but prolonged surge of 0.5–0.6 m occurred over a time span of 3½ days. The morphological response was more significant during this experiment. The inner subtidal bar migrated onshore, welded to the beach and transformed into an intertidal swash bar while a new subtidal bar formed further seaward (Figure 3).

During SK96, the inner subtidal bar was linear and no cell circulations involving rip currents were observed over this bar (Figure 4). The overall energy levels were generally higher during SK96. A series of 10 storms occurred over a three-week period and significant wave heights in the outer nearshore were up to 2.85 m with peak spectral periods of 13.5 seconds during an intense storm which resulted in a 2.08 m storm surge. Other surges ranged from 0.5–1.5 m in elevation. This high-energy period resulted in intertidal swash bar erosion and reformation at a lower level, while the inner subtidal bar migrated landward (Figure 3).

In Table 1, the aspect ratio of the inner subtidal bar has been listed for all three experiments. The aspect ratio is here defined as the ratio of bar height to distance between the deepest point of the inner trough and the inflection point on the seaward bar slope. While the ratio is generally small at Skallingen, it increased substantially during the SK96-experiment. Table 1 also contains data from a number of beaches described in the literature. The data suggest that this ratio decreases with increasing spring tidal range and with decreasing nearshore slope.

RESEARCH METHODS AND DATA ANALYSIS

As illustrated in Figure 3, five or six instrument stations were deployed in cross-shore transects spanning the intertidal and upper subtidal zones during all three experiments. These stations were each equipped with one Marsh McBirney OEM512 electromagnetic current meter and three optical backscatter sensors (OBS-1P), the latter being installed at nominal elevations of z = 0.05, 0.10 and 0.20 meters above the bed. The current meters were generally installed 5–10 cm above the level of the upper OBS. While the OBS were deployed close to the bed to capture significant sediment suspensions, the current meters were kept further away in order to minimize the risk of burial and signal distortion from the boundary. The elevations of the instruments were adjusted at each low tide, if possible, to compensate for bed level changes.

Pressure sensors were installed at the seaward-most instrument station (S1) and in the mid-lower intertidal zone (at S5 during SK94 and SK95; at S4 during SK96). All sensors were cable-linked to a shore-based data acquisition system and sampled at 4 Hz for periods of 34.1 minutes during recording events. Instrument runs were spaced 1–1.5 hours apart. At distances of 500–800 m from the shoreline and seaward of the bars (Figure 2), a Pacer Model WTG10688 pressure sensor was installed; this instrument sampled incident waves at 2 Hz for periods of 17 mins every 2 hours, as well as mean water levels at intervals of 7.5 minutes.

Instrument outputs were screened and checked for data quality. Noisy and/or erroneous data were discarded. Such errors could occur when instruments were exposed to air (manifested as virtually instantaneous drops to zero current velocities), or buried. With respect to the backscatter sensors, the concentration profiles sometimes became inverted in very shallow water depths, with large spikes occurring during the passage of wave crests. Such signals were interpreted as being due to bubbles injected into the water column and records were subsequently discarded. Signals from the backscatter sensors were gain-calibrated in a recirculating tank using sand from the deployment locations while field offsets were determined for individual records using the 5th percentile frequency output voltage (see AAGAARD and GREENWOOD, 1994). Net suspended sediment flux at a point was computed as the cross-product of instantaneous velocity (u) and sediment concentration (c):

$$\langle q_s \rangle = \frac{1}{n} \sum uc \tag{8}$$

where n is the number of data points in the sample and $\langle\rangle$ denotes the time-average. Following JAFFE *et al.* (1984) and HUNTLEY and HANES (1987), the net flux was separated into a mean and an oscillatory term:

$$\langle q_s \rangle = \overline{uc} + u'c' \tag{9}$$

where the first term on the right-hand side of the equation is flux due to mean currents, and the second term is due to oscillatory wave motion. Information on transport magnitude and direction across frequency space was obtained from plotting the cospectra of velocity and concentration, and using

$$u'c' = \frac{\Delta f}{F} \sum C_{uc}(f) \quad (10)$$

where $C_{uc}(f)$ is cospectral density at a given frequency, Δf is cospectral resolution and F cospectral frequency range, in this case 2 Hz (HUNTLEY and HANES, 1987). Sediment flux contributions from incident and infragravity waves were separated at a cospectral frequency of 0.067 Hz. Sediment flux at a given station was evaluated from the lowermost exposed sensor in an array. Integrations over an instrument array were not performed because a) results have shown that the two estimates are proportional; sediment flux reversals at increasing elevations above the bed are extremely rare over the bars at Skallingen and b) due to bed level changes, the distance between sensors and the bed often varied significantly particularly during SK96, rendering vertical integrations meaningless, particularly in the case when a sensor became buried. Surface elevation spectra were computed from pressure records and corrected for frequency-dependent depth-attenuation using linear wave theory

$$S_s(f) = \left(\frac{\cosh kh}{\cosh k(z + h)}\right)^2 S_p(f) \quad (11)$$

(BISHOP and DONELAN, 1987), where $S_s(f)$ is surface elevation spectral density at frequency f, $k = 2\pi/L$, z is depth of submergence of the pressure transducer and S_p is measured pressure spectral density. Root-mean-square wave heights were estimated over the frequency range 0.0–0.4 Hz and computed as

$$H_{rms} = \sqrt{8}\left(\sum S_s(f)\right)^{1/2} \quad (12)$$

and significant wave heights were determined as $H_s = 1.414\ H_{rms}$. The surface elevation spectra were separated into infragravity wave (0–0.067 Hz) and incident wave (0.067–0.4 Hz) components. Wave heights at stations lacking pressure sensors were estimated from current meter variance using a linear transfer function

$$H_{rms} = \sqrt{8}(<\sigma^2> h/g)^{0.5} \quad (13)$$

(THORNTON and GUZA, 1989a), where σ^2 is velocity variance, h is water depth and g the acceleration due to gravity. Oscillatory velocities were separated into incident and infragravity wave band contributions using Fourier filtering techniques and using a frequency cut-off of 0.067 Hz.

Morphological changes were determined using cross-shore arrays of survey stakes, spaced 5 m apart. The level of the bed relative to the top of the rods was recorded at each low tide throughout the experiments (except when the stakes were inaccessible). This method was supplemented by conventional surveying techniques using total stations and echosounding in 4–7 transects spaced 50 m apart.

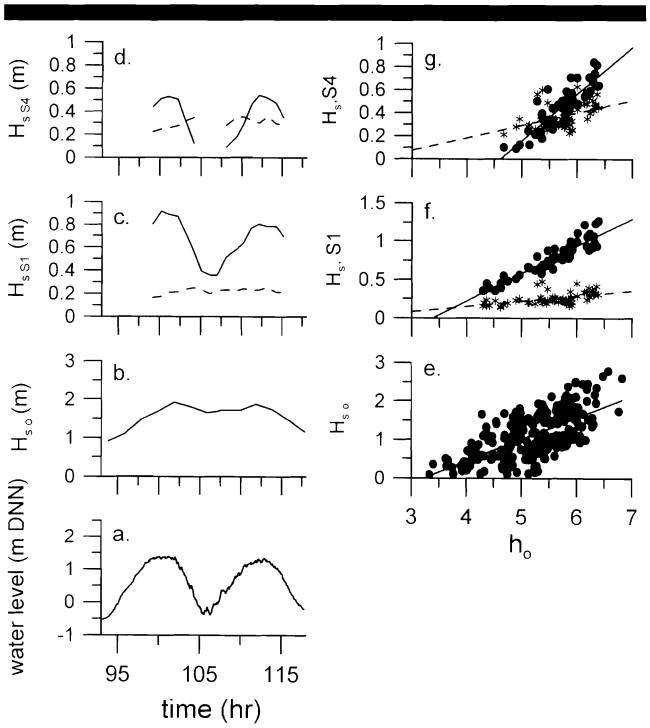

Figure 5. Wave heights recorded during SK96. The panels show: a) mean water level, and b) significant wave height recorded offshore, c) significant incident (solid line) and infragravity (dashed) wave heights at S1, and d) at S4. The regressions show significant incident (solid) and infragravity (dashed) wave heights, plotted against offshore water level at e) the offshore wave recorder, f) S1 and g) S4.

RESULTS AND DISCUSSION

In this section, hydrodynamic parameters (incident and infragravity wave heights, incident wave asymmetries, mean current velocities) as well as net suspended sediment transport rates will be tested for dependence upon water depth. In the present experiments, changes in water depth were mainly induced by tidal fluctuations but also depended upon storm surge elevations. Obviously, factors other than water level, *e.g.* deepwater wave height, period, wave incidence angle, wind speed and direction, prevailing bathymetry at the field site as well as bed configuration will have profound effects upon the characteristics of nearshore hydrodynamics and sediment transport. Consequently, a relatively large degree of scatter in the tested relationships is to be expected a priori. In the following figures, response has been plotted against forcing to test for linear trends within a given dataset (SK94, SK95 and SK96, respectively) and data in the time domain have been included for visual assessment. All illustrated regressions were significant at the 1%-level.

Wave Parameters

In Figure 5, wave heights within (S1, S4) and seaward of the surf zone have been linearly regressed against local water depth during SK96. The time series indicate that incident wave heights increase at high tide and this is confirmed by the regressions. Offshore wave heights display a surprisingly

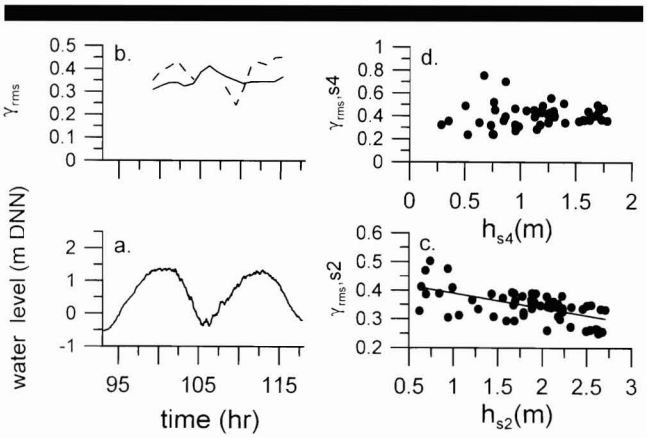

Figure 6. Breaker ratios recorded during SK96. a) Mean water level, b) γ_{rms} at S2 (solid line) and S4 (dashed line) during two tidal cycles. In c) and d), γ_{rms} has been plotted against local water depth at S2 and S4, respectively, for the entire dataset.

strong correlation with local water depth (r^2 = 0.430). This would suggest that wave heights seaward of the surf zone are dependent upon the amount of frictional loss across the shallow offshore (eq. 1) which should increase with decreasing water depth. However, at this field site large wave heights usually occur in combination with strong onshore winds, generating storm surges and the effect of water level cannot be clearly separated from the generally high-energy conditions at times of large water depths.

Nearshore data were collected during moderate-high energy conditions when incident waves generally broke on the outer subtidal bar (Figure 2), partly reformed in the trough and broke again on the lower seaward slope of the inner bar, the exact location depending upon tidal stage. Contributions from incident and infragravity waves at S1 and S4 have been separated in Figure 5 and at fixed locations within the surf zone, incident wave heights were highly correlated with water depth (S1: r^2 = 0.865; S4: r^2 = 0.763) due to depth-dependent wave breaking over the bars (eq. 3). In contrast, infragravity waves were not strongly correlated with water depth (r^2 = 0.272 and 0.192 at S1 and S4, respectively). Over the inner bar (S1), incident wind waves dominated the energy spectrum at all times while infragravity energy was more significant in the intertidal zone at low tidal stages ($h_{S4} < \sim$ 1 m) due to the dissipation of incident waves and the amplification of infragravity energy close to shore (Figure 5g).

Figure 6 illustrates the local breaker ratio, γ_{rms}, computed from high-pass filtered records. Thus, only incident wave heights are considered. At S4, γ was independent upon water depth and on the order of 0.4 (Figure 6d). Hence, incident waves were usually saturated at S4 and this station was mostly located in the inner surf zone, irrespective of tidal stage. At the bar crest (S2), γ was negatively correlated with h (r^2 = 0.348). The breaker ratio and hence local wave energy dissipation increased with decreasing water depth but remained above 0.23 at all times. Therefore, the bar crest tended to be located in the inner surf zone at low tide and in the outer surf zone at high tide.

As noted above, incident wave asymmetry is a major source for onshore transport of sediment and is expected to be at a maximum at the breakpoint and decrease into the surf zone. Consequently, incident wave asymmetry should be modulated at tidal frequencies at fixed points within the surf zone, as the breakpoint moves back and forth. Here, incident wave asymmetry (a) was evaluated at the bar crest (S2) and computed as

$$a = \frac{(u_c^3 - u_t^3)}{(u_c^3 + u_t^3)} \quad (14)$$

(VAN RIJN, 1993) where u_c,u_t are the high-pass filtered maximum oscillatory velocities at wave crests and wave troughs, respectively. Figure 7 illustrates that incident wave asymmetry at the inner bar did increase with water depth (r^2 = 0.685). The asymmetry was invariably positive, *i.e.* directed onshore.

Nearshore Currents

Across the inner subtidal bar (S1 and S2), there was no correlation between longshore current velocity and water depth probably because of the effect of wave incidence angle (eq. 5) and the fact that wave heights and hence wave energy gradients were not strongly depth-dependent when these stations were located in the outer surf zone (high water levels). In the intertidal zone (S4 and S5) where incident waves were strongly refracted, a relationship did exist between h and V (Figure 8) with maximum current velocities at high tide (r^2 = 0.307).

During SK96, the bathymetry was homogeneous alongshore and no rip current circulations were observed. Consequently, cross-shore currents were due mainly to undertow. The influence of bathymetric changes is expected to blur any expected relationships between water depth and current velocity as wave height gradients depend on local bed gradients. However, significant relationships did exist (Figure 9) with undertow velocities increasing for decreasing water depths over the inner subtidal bar (S2; r^2 = 0.375, Figure 9d) and the opposite tendency in the intertidal zone (S4; r^2 = 0.139, Figure 9e) where undertow velocities peaked during high water levels. The former is probably due to increased local wave dissipation over the bar at low water levels when waves became saturated (Figure 6); maximum current velocities occurred for large values of γ (Figure 9h; r^2 = 0.230). The increasing undertow velocities with increasing water levels observed at S4 were associated with generally increasing negative wave energy gradients across the surf zone at high tide. Figure 9g shows a clear relationship between wave energy gradient and undertow velocity, recorded at S4 with a coefficient of determination r^2 = 0.373. At S2, a connection between the undertow velocity and $\delta H^2/\delta x$ could not be identified as the secondary wave breakpoint was frequently located between S1 and S2.

At Skallingen, horizontally-segregated mean flows involving onshore-directed currents across bars and offshore-directed rip currents in gaps between bars frequently replace undertows. Rip currents also tend to be modulated by changing water depths with maximum current velocities occurring

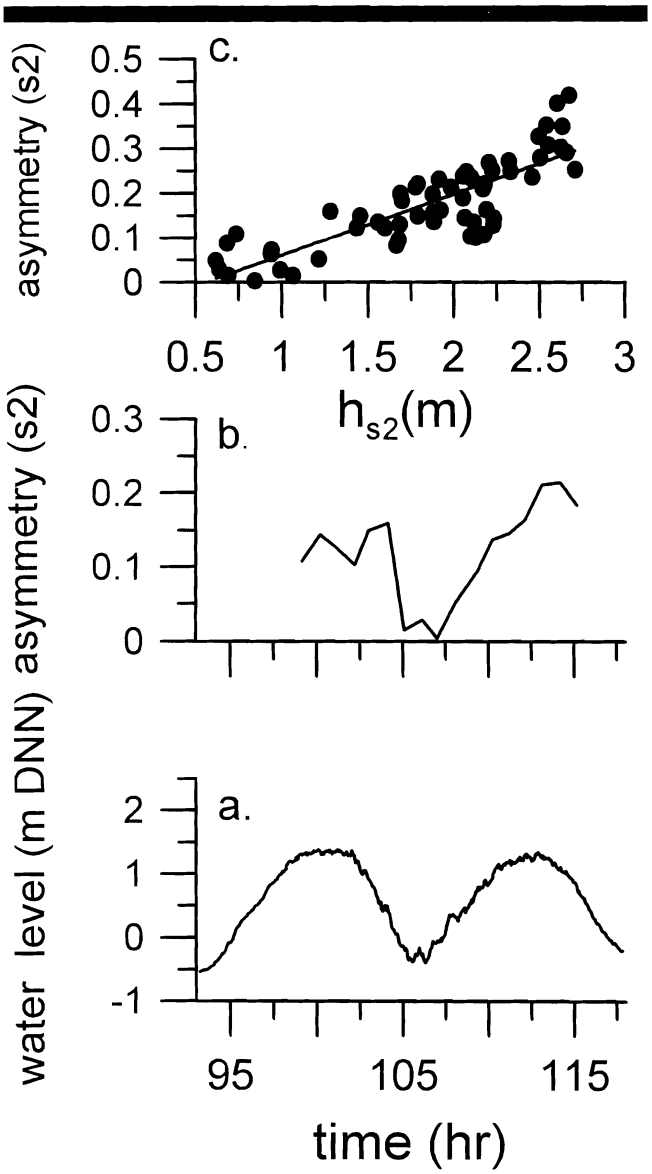

Figure 7. Incident wave asymmetries during SK96. a) Mean water level and b) incident wave asymmetry at S2 during two tidal cycles. Panel c) illustrates asymmetry at S2 plotted against local water depth for the entire dataset.

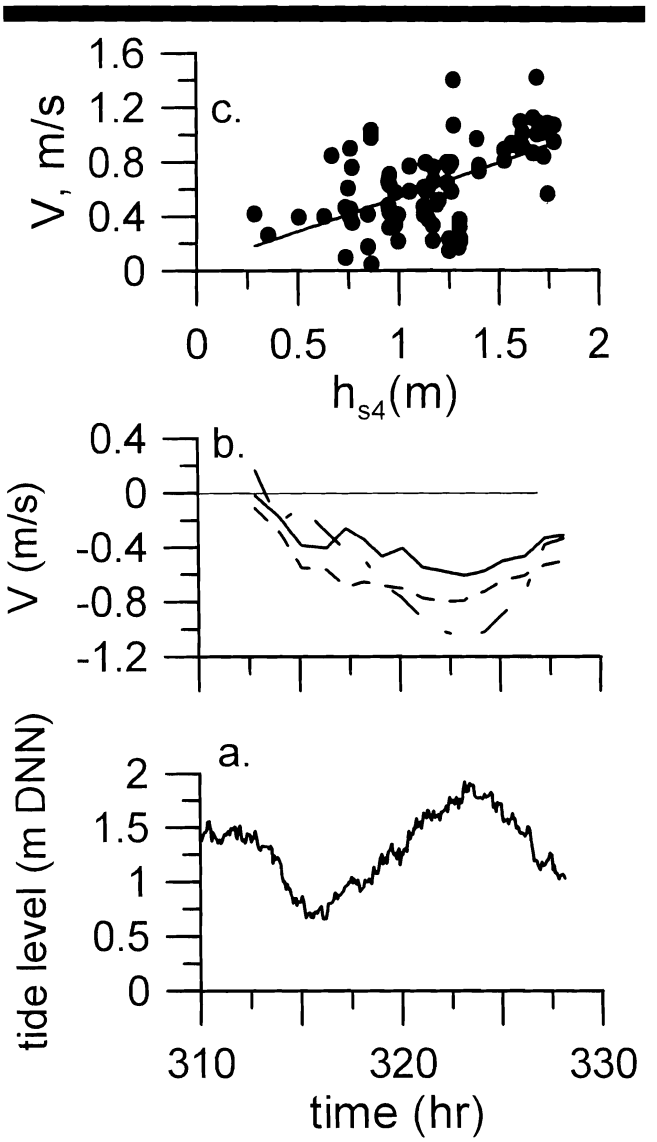

Figure 8. Longshore current velocities during SK96. a) Mean water level, b) longshore current velocity at S2 (solid), S4 (dashed) and S5 (dash-dot) for a selected time period. c) illustrates longshore current velocities at S4 and S5 regressed against water depth at S4.

at times of low tide (AAGAARD *et al.*, 1997; BRANDER, 1999). Figure 10 provides an example from SK94 when mean current velocities were recorded at S2 located in the rip neck. In the example from the time domain, rip velocities were essentially a mirror-image of the water level curve and the regression confirms that rip velocities were inversely related to water depth (r^2 = 0.748; Figure 10c). Similar to undertows in the subtidal zone, rip current speeds peaked at low tide. This was probably due either to increased local wave energy dissipation at low tide (Figure 10d; r^2 = 0.412) and/or increasing topographic constriction in the rip neck (BRANDER, 1999).

Rip currents are fed by onshore directed mean flows across the bar crest between rip channels. Theoretically, these flows are not measureable using electromagnetic current meters, as Stokes drifts are Lagrangian flows and mass transport due to the wave rollers are thought to be confined within the region between wave crest and wave trough (*e.g.* SVENDSEN, 1984). However, during SK95 when the instruments were deployed across the inner bar between two rip channels, a well-defined rip circulation was initiated with rip channels spaced 350–400 m apart (Figure 4). Contrary to expectations, an almost persistently onshore directed mean current developed across the crest of the inner bar. While the exact source of these onshore-directed flows is a moot point, maximum current speeds were again observed at low tidal stages (Figure 11; r^2 = 0.420).

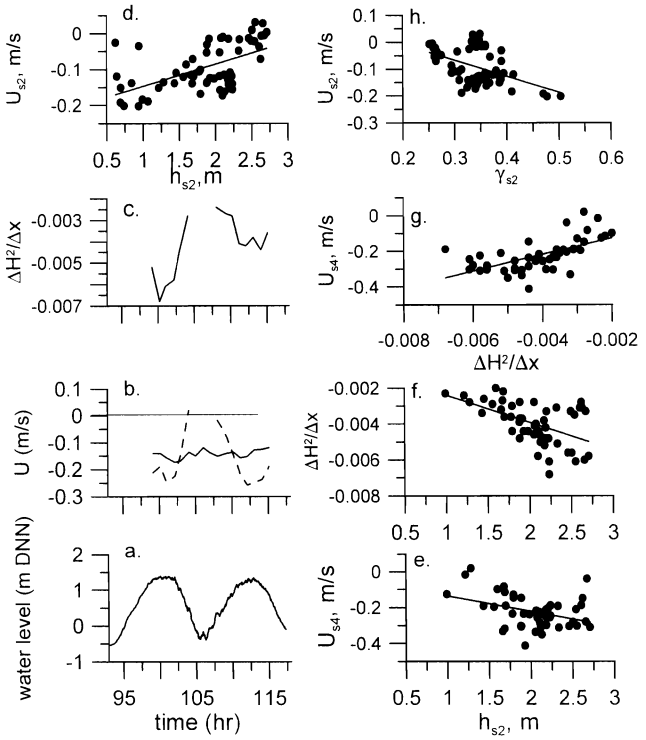

Figure 9. Cross-shore currents during SK96. a) mean water level, b) cross-shore currents at S2 (solid) and S4 (dashed), and c) cross-shore wave energy gradients between S2 and S4, for a selected time period. The remaining panels illustrate cross-shore current velocity at S2 (d) and S4 (e), and wave energy gradient (f) as a function of water level, g) is cross-shore current velocity at S4 as a function of wave energy gradient, and finally h) is cross-shore velocity at S2 as a function of the local breaker ratio.

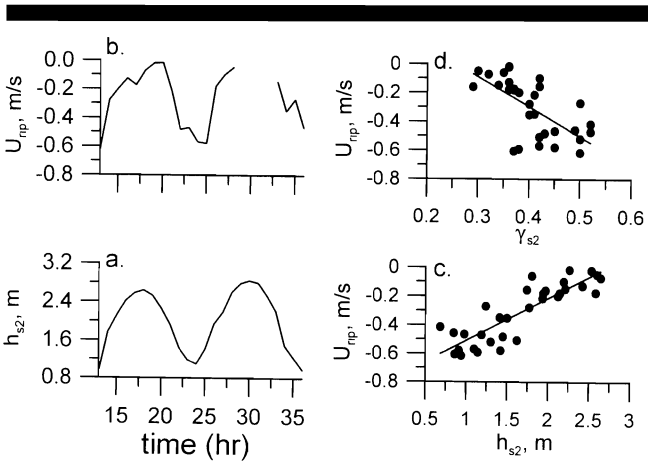

Figure 10. Rip current velocities during SK94. The figure illustrates a) water depth at S2 and b) associated rip current velocities for a selected time period, as well as rip current velocity plotted against water depth (c) and local breaker ratio (d) for the entire dataset.

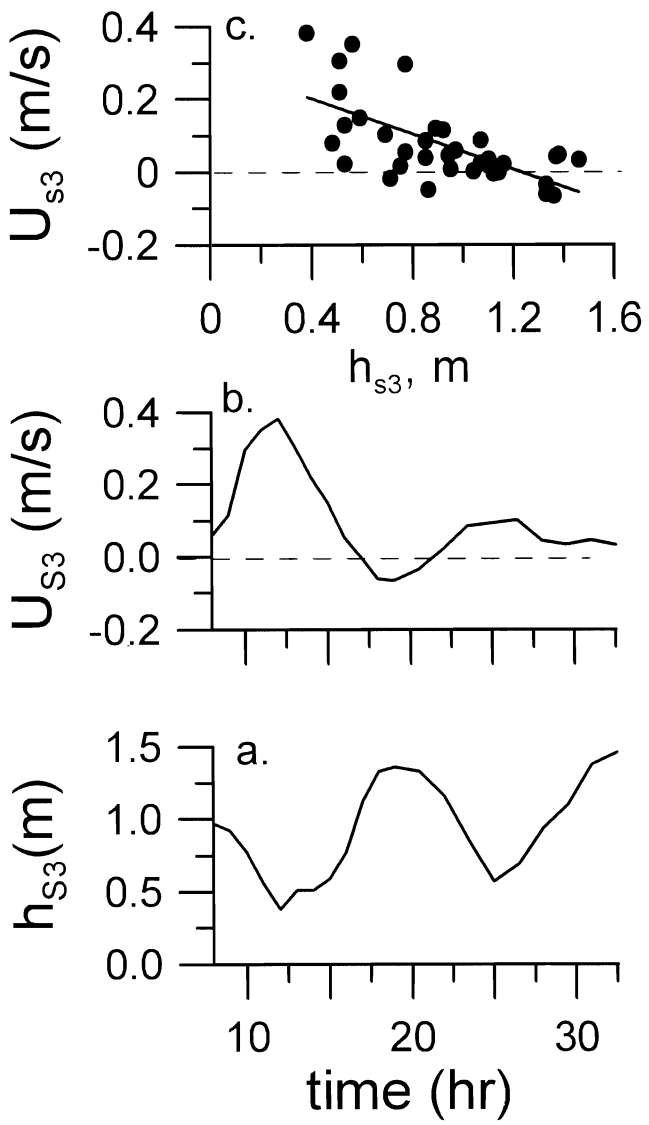

Figure 11. Cross-shore currents during SK95. a) Mean water depth at the bar crest and b) associated cross-shore current velocity during a selected period of time. c) illustrates current velocity against water depth for the entire dataset.

Suspended Sediment Transport

Suspended sediment transport is a function of the concentration of suspended sediment, skewnesses in the ambient velocity field (which may be due to either oscillatory velocity asymmetries or mean currents superimposed on a symmetrical orbital motion), and the cross-correlation and phase relationship between velocity and concentration. Over flat beds, the phase lag of the sediment concentration relative to the applied forcing is generally small close to the bed and increases with elevation owing to the finite time it takes for the sediment to diffuse upwards (*e.g.* RIBBERINK and AL-SALEM, 1995). Over rippled beds, phase lags between velocity and sediment concentration are generally larger and in some cas-

es up to 180 degrees as sediment resuspension occurs as a convective process with sediment-laden vortices being shed from ripples at times of velocity reversals (*e.g.* OSBORNE and GREENWOOD, 1993). In the surf zone at Skallingen, the bed is generally flat at times of high energy due to the fine grain sizes, except in troughs and rip channels where megaripples may exist.

The amount of sediment suspended into the water column for a given bed configuration mainly depends upon the bed shear stress and the macroturbulence generated by wave breaking. Wave-induced bed shear stresses are usually significantly larger than shear stresses due to mean current velocities. This is due in part to generally larger orbital than mean velocities, as well as differences in boundary layer thickness and hence velocity gradient near the bed. Sediment concentrations in the surf zone are therefore expected to respond mainly to changes in oscillatory velocity and thus local wave height. As wave height is dependent upon water depth (Figure 5), suspended sediment concentration should also vary with the tidal stage.

Such a trend is difficult to verify with the equipment used here, as sediment concentration gradients are steep close to the bed, and the distance between the bed and a given OBS-sensor will change as the bed erodes/accretes. During SK95, however, net bed elevation changes between successive low tides (when the sensors were adjusted) were relatively small at the inner bar crest (S3; Figure 3), on the order of 5 cm. Figure 12 illustrates sediment concentration recorded at the lower OBS at a nominal elevation of z = 0.05 cm. Visually, it appears that a relationship does exist with sediment concentrations exceeding 1.5 g/l at high tide, decreasing to approximately 0.75 g/l at low tide but the predictive relationship is weak ($r^2 = 0.147$).

Morphological change (*e.g.* nearshore bar migration and changes in profile configuration) depends mainly upon cross-shore sediment transport gradients. It is difficult to predict how cross-shore transport patterns will respond to changes in water level because net transports consist of significant contributions from both mean currents and oscillatory waves at incident and infragravity frequencies (*e.g.* BEACH and STERNBERG, 1991; OSBORNE and GREENWOOD, 1992), the characteristics of which tend to display different trends with changes in water depth, as illustrated above.

Figure 13 shows sediment flux measurements in the inner surf zone (S4) during SK96 when the cross-shore currents were undertows and the data illustrate a tendency for the net sediment flux to be large and directed offshore when water levels were high, and smaller and/or directed onshore towards low tide (Figure 13g; $r^2 = 0.227$).

From an assessment of the individual transport constituents, the mean flux increased with water depth ($r^2 = 0.190$) due to increasing undertow velocities (Figures 9 and 13d). Onshore directed flux due to incident waves similarly increased in relatively large water depths but was significantly smaller than the mean flux and no predictive relationship ($P < 0.01$) with the water level existed. One of the reasons for the lack of correlation may be the thin boundary layer associated with incident waves and the associated large gradients of vertical mixing, rendering flux estimates extremely sensitive to sensor elevation above the bed. Another contributing factor could be variations in local bed shear stress leading to (subtle) variations in bed configuration which would influence phase coupling between oscillatory velocity and sediment concentration (AAGAARD and GREENWOOD, 1999). Sediment flux due to oscillatory infragravity motion was almost consistently directed onshore at this location and it was the reason for the few cases of onshore directed net flux observed in small water depths ($h < 0.8$ m) even though a predictive relationship did not exist at the 0.01 significance level. Hence, in the intertidal zone, net sediment transport tended to be directed offshore due to mean flows during high tide and storm surges while there was a tendency for onshore di-

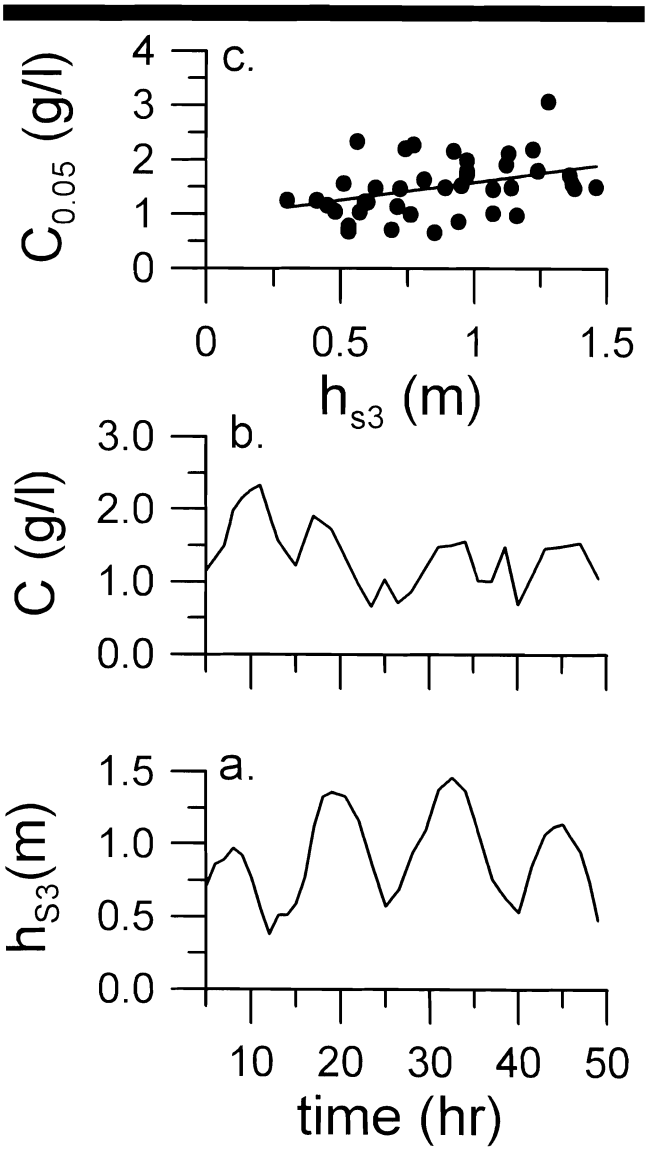

Figure 12. Sediment concentrations at the bar crest (z = 0.05 m) during SK95. a) Mean water depth and b) sediment concentration at the bar crest for a selected period of time. c) is concentration as a function of water depth for the entire dataset.

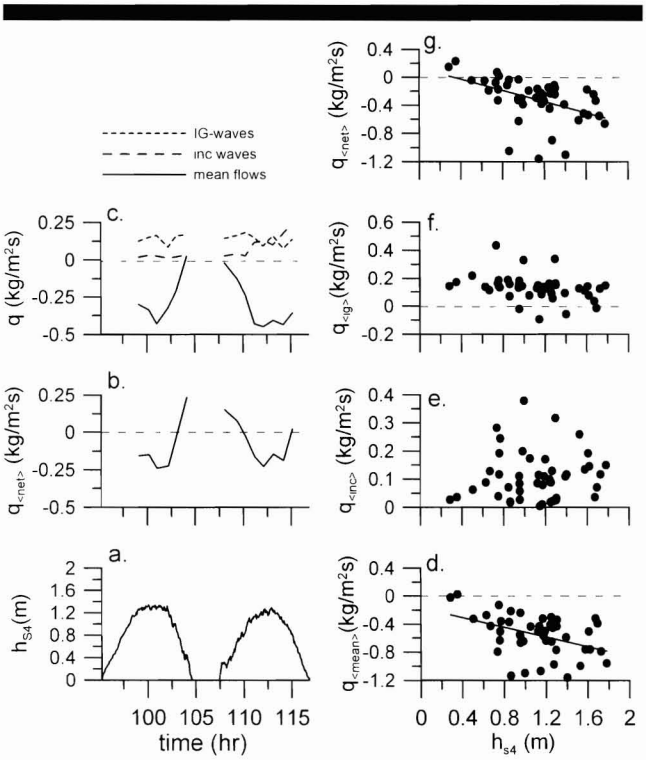

Figure 13. Cross-shore sediment flux in the inner surf (intertidal) zone during SK96. The panels show a) water depth at S4, b) net suspended sediment flux and c) sediment flux due to mean currents, incident and infragravity waves during two tidal cycles. Panels (d)-(g) illustrate mean flux, incident wave and infragravity flux, and finally net flux, plotted as a function of local water depth for the entire dataset. Note the differences in vertical scale.

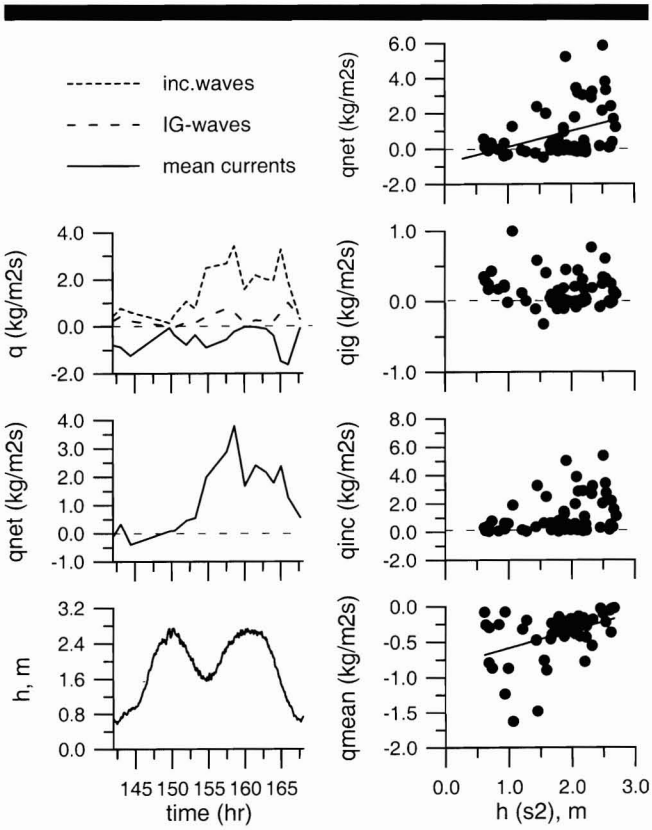

Figure 14. Cross-shore sediment flux recorded at the crest of the inner subtidal bar (S2) during SK96. The panels show a) water depth at S4, b) net suspended sediment flux and c) sediment flux due to mean currents, incident and infragravity waves during two tidal cycles. Panels (d)–(g) illustrate mean flux, incident wave and infragravity flux, and finally net flux, plotted as a function of local water depth for the entire dataset. Note the differences in vertical scale.

rected sediment flux driven by infragravity wave motions at low tide.

At the nearshore bar, these trends in sediment flux were reversed. Onshore directed, and occasionally large, sediment fluxes occurred during high water levels, while the tendency was for smaller and offshore directed fluxes when water levels were low (Figure 14) even though the correlation was barely significant at 1% (r^2 = 0.129, Figure 14g). Offshore sediment flux at low tide was due to the undertow (Figure 14d), while onshore flux at high tide was due to the incident waves (Figure 14e).

Infragravity fluxes were again generally onshore but were small and did not depend upon water depth. Similarly, a predictive relationship involving the incident waves did not exist and this produced a significant amount of scatter in the relationship between water depth and net flux. The plot of incident wave flux against water depth (Figure 14e) shows a number of very large flux rates which were associated with three large surges towards the end of SK96. These enhanced onshore directed fluxes at incident wave frequencies were mainly due to dramatically increased bed shear stresses, significantly improving the phase-coupling between oscillatory velocity and sediment concentration (AAGAARD and GREENWOOD, 1999); as a consequence, net sediment fluxes did not reverse during the tidal cycles encompassed by these surges. Figure 14a-c depicts the water level and sediment fluxes at the inner subtidal bar during one of these surges.

Finally, in the rip channel, Figure 15 illustrates that net sediment fluxes were again directed offshore at low tide due to increasing rip velocities (r^2 = 0.529; Figure 15g), while onshore fluxes due to incident wave activity prevailed at higher water levels. In this case, infragravity wave fluxes were mainly directed offshore, but again there was no relationship with water depth.

SUMMARY DISCUSSION

The examples illustrated above have indicated that changing water levels, induced by *e.g.* tides and/or storm surges may be an important factor in modulating surf zone hydrodynamics and sediment transport. It is clear that other mechanisms may be equally or more important, such as offshore wave conditions and surf zone bathymetry. Such factors may provide systematic or unsystematic deviations from the tendencies and trends induced by the variations in water level. Therefore, in many cases the relationships between process (water level change) and response were weak. This was par-

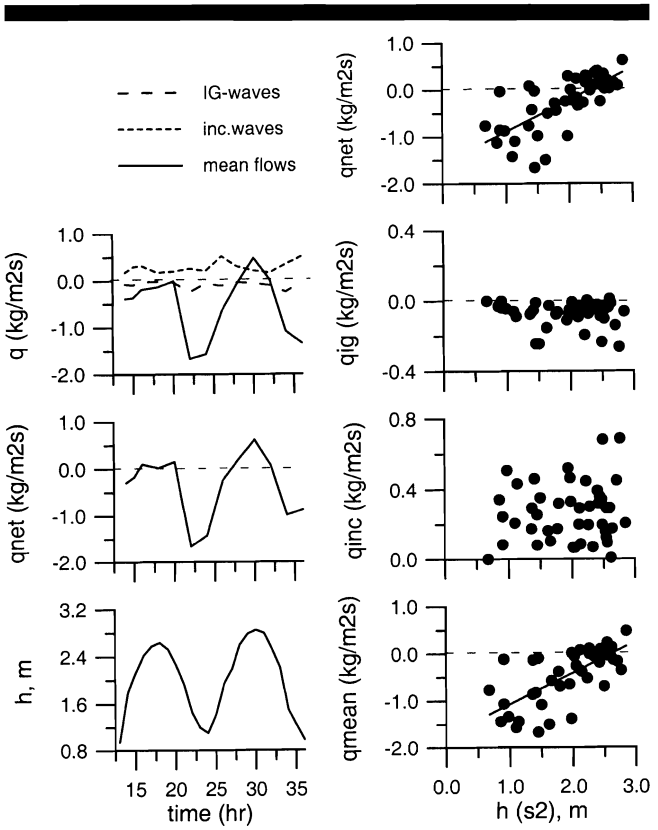

Figure 15. Cross-shore sediment flux in a rip channel (S2) during SK94. The panels show a) water depth at S2, b) net suspended sediment flux and c) sediment flux due to mean currents, incident and infragravity waves during two tidal cycles. Panels (d)–(g) illustrate mean flux, incident wave and infragravity flux, and finally net flux, plotted as a function of local water depth for the entire dataset.

ticularly the case with respect to sediment concentration and transport predictions and there are at least two major reasons for the increased amount of scatter in these cases. One is the inherent limitations of the measurement technique. Suspended sediment concentrations and thus sediment flux were evaluated at fixed points within the water column. The distance between the bed and the sensors varied over time, introducing significant changes in the amount of sediment 'seen' by a given sensor. The second is the possibility of changes in bed configuration, resulting in variable degrees of phase coupling between velocity at incident wave frequencies and sediment concentration at given elevations. Despite these reservations, viewed over a range of conditions, it would appear that changing water levels may be of importance to hydrodynamics, sediment transport, and ultimately profile change.

With respect to the sediment flux, the observed trends were the following: In the subtidal zone, there was a tendency towards onshore flux at high water levels, driven by the incident waves and towards offshore flux at low tide due to mean currents (undertow/rip currents). In the intertidal zone, this trend was reversed. At high tide, there was a tendency towards offshore flux due to mean currents, while in small water depths, undertow velocities decreased, incident wave energy was largely dissipated and the net sediment flux tended to be directed onshore, mainly due to infragravity waves.

Except in rip channels, sediment flux due to oscillatory infragravity waves was almost exclusively directed onshore. This was also the case in the intertidal zone (Figure 13f) which is contrary to most reports in the literature. BEACH and STERNBERG (1991), BUTT and RUSSELL (1999) and RUSSELL and HUNTLEY (1999) all observed offshore directed infragravity transport in the inner surf/swash zones due to negative velocity asymmetries and/or phase shifts between velocity and sediment concentration. There is obviously a need for more research on sediment transport due to infragravity waves under a range of conditions.

The results obtained here indicate that sediment transport directions within the surf zone may change over tidal cycles, as a function of changing water levels. Due to the existence of morphological lags, such directional changes (*e.g.* offshore transport at low tide and onshore at high tide) would be expected to lead to a smoothing of bar relief. Indeed, the bars at Skallingen are characterized by smaller aspect ratios than bars subjected to smaller tidal ranges and/or occurring on steeper nearshore slopes (Table 1). An exception is the bar configuration towards the end of SK96 when the subtidal bar increased significantly in relief. As discussed above, the latter was associated with a lack of observed sediment flux reversals over a number of large storm surges; recorded sediment flux was exclusively directed onshore. Such tendencies for bar smoothing due to varying sediment transport directions over tidal cycles will be more significant for beaches subjected to large TR/β-ratios as transport reversals occur over larger vertical and horizontal (cross-shore) distances. These tendencies should also result in less overall bar mobility, *i.e.* rather low, broad and stable bars (and rip channels) compared to sites where sediment transports are unidirectional over longer periods of time. With more stable transport patterns over longer time spans, the phase lag between forcing and morphological response will become smaller and bars should become more mobile and steeper, as illustrated by the example from SK96.

Extending these observations to longer time scales, consistently increasing water levels would be expected to result in an erosion of the beach/intertidal zone and a tendency for the subtidal bars towards moving onshore, as was observed in the morphological studies by HANDS (1977). With a decreasing water level, subtidal bars should move offshore while the intertidal zone will tend to accrete, *e.g.* by swash bar formation and growth.

Finally, it should be emphasized that the present results were all obtained under relatively high-energy conditions at locations within the surf zone. Hence, the observed sediment transport tendencies were not simply due to lateral shifts of the shoaling/surf/swash zones as a function of tidal stage or energy level.

CONCLUSIONS

In conclusion, this study has provided quantitative evidence for the effect of changes in water depth (due to tides and storm surges) upon surf zone hydrodynamics and sedi-

ment transport. Physical processes capable of explaining topographic smoothing and stability on beaches subjected to significant tidal fluctuations have been identified. It was found that high water levels were associated with large offshore and surf zone incident wave heights, probably due to less frictional dissipation offshore and to decreasing incident wave saturation at a given point within the surf zone. Increased water levels also resulted in increased (negative) wave energy gradients between the subtidal bar and the beach, and hence increased mean current velocities in the inner surf (intertidal) zone where incident waves were always saturated. Mean currents increased over the subtidal bar for low water levels, due to increased local incident wave dissipation. Sediment flux patterns were modulated by the changing water levels. With a high mean water level, the flux tended to be directed offshore in the intertidal zone and onshore in the subtidal zone, while these trends were reversed with low mean water levels. When such sediment flux trends occur at tidal frequencies they will tend to smooth bar forms due to morphological lags, producing relatively stable bars with a small aspect ratio. When they occur at lower frequencies where morphological lags attain less importance and the stochastic nature of wave forcing and bathymetric conditions average out, they may induce predictable and systematic cross-shore profile changes.

ACKNOWLEDGEMENTS

This research was supported by the Danish Natural Sciences Research Council, grant nos. 11-0925 and 9701836. Jørgen Nielsen, Niels Nielsen, Rasmus N. Nielsen, Kalle Kronholm, Christian Helledie and Carlo Sørensen (Univ. Copenhagen), Brian Greenwood, Carl Boldy and Kitty Brown (Univ. Toronto) shared the long nights on the beach. A special thanks to our electronics wizard, Ulf Thomas. The comments and suggestions by the journals' referees significantly improved the contents and scope of this paper.

LITERATURE CITED

AAGAARD, T. and GREENWOOD, B., 1994. Suspended sediment transport and the role of infragravity waves in a barred surf zone. *Marine Geology*, 118, 23–48.

AAGAARD, T. and GREENWOOD, B., 1995. Suspended sediment transport and morphological response on a dissipative beach. *Continental Shelf Research*, 15, 1061–1086.

AAGAARD, T and GREENWOOD, B., 1999. Directionality of cross-shore sediment transport in the surf zone under high-energy conditions. *In:* KRAUS, N.C. and MCDOUGAL, W.G. (ed) *Coastal Sediments '99*, American Society of Civil Engineers, pp.1003–1018.

AAGAARD, T.; GREENWOOD, B., and NIELSEN, J., 1997. Mean currents and sediment transport in a rip channel. *Marine Geology*, 140, 25–45.

AAGAARD, T.; NIELSEN, N., and NIELSEN, J., 1994. Cross-shore structure of infragravity standing wave motion and morphological adjustment: an example from Northern Zealand, Denmark. *Journal of Coastal Research*, 10, 716–731.

BATTJES, J.A. and JANSSEN, J.P.F.M., 1978. Energy loss and set-up due to breaking of random waves. *Proceedings 16th International Conference on Coastal Engineering*, American Society of Civil Engineers, pp.569–587.

BEACH, R.A. and STERNBERG, R.W., 1991. Infragravity driven suspended sediment transport in the swash, inner and outer surf zone. *In:* KRAUS, N.C.; GINGERICH, K.J., and KRIEBEL, D.L. (ed) *Coastal Sediments '91*, American Society of Civil Engineers, pp. 114–128.

BISHOP, C.T. and DONELAN, M.A., 1987. Measuring waves with pressure transducers. *Coastal Engineering*, 11, 309–328.

BOWEN, A.J., 1969. The generation of longshore currents on a plane beach. *Journal of Marine Research*, 27, 206–215.

BRANDER, R.W., 1996. Field observations on the morphodynamics of rip currents. Unpubl.Ph.D. thesis, Department of Geography, University of Sydney, 240pp.

BRANDER, R.W., 1999. Field observations on the morphodynamic evolution of a low-energy rip current system. *Marine Geology*, 157, 199–217.

BRETSCHNEIDER, C.L. and REID, O.R., 1954. *Modification of wave height due to bottom friction, percolation and refraction.* Beach Erosion Board, Tech. Memo 45, U.S. Army Corps of Engineers, 36pp.

BUTT, T. and RUSSELL, P., 1999. Suspended sediment transport mechanisms in high-energy swash. *Marine Geology*, 161, 361–375.

DALLY, W.R. and OSIECKI, D.A., 1995. The role of rollers in surf zone currents. *Proceedings 24th Coastal Engineering Conference*, American Society of Civil Engineers, pp.1895–1905.

DAVIDSON, M.A.; RUSSELL, P.E.; HUNTLEY, D.A., and HARDISTY, J., 1993. Tidal asymmetry in suspended sand transport on a macrotidal intermediate beach. *Marine Geology*, 110, 333–353.

DAVIS, R.A.; FOX, W.T.; HAYES, M.O., and BOOTHROYD, J.C., 1972. Comparison of ridge and runnel systems in tidal and non-tidal environments. *Journal of Sedimentary Petrology*, 42, 413–421.

DOERING, J.C. and BOWEN, A.J., 1985. Skewness et al.; the spatial distribution of some moments of the nearshore velocity field. *Proceedings Canadian Coastal Conference 1985*, pp. 5–16.

FEDDERSEN, F.; GUZA, R.T.; ELGAR, S., and HERBERS, T.H.C., 1997. Cross-shore structure of longshore currents during Duck 94. *Proceedings 25th International Conference on Coastal Engineering*, American Society of Civil Engineers, pp.3666–3679.

GUZA, R.T. and THORNTON, E.B., 1982. Swash oscillations on a natural beach. *Journal of Geophysical Research*, 87, 483–491.

HANDS, E.B., 1977. Implications of submergence for coastal engineers. *Proceedings Coastal Sediments '77*, American Society of Civil Engineers, pp. 149–166.

HUNTLEY, D.A. and HANES, D.M., 1987. Direct measurement of suspended sediment transport. *Coastal Sediments '87*, American Society of Civil Engineers, pp. 723–737.

JAFFE, B.E.; STERNBERG, R.W., and SALLENGER, A.H., 1984. The role of suspended sediment in shore-normal beach profile changes. *Proceedings 19th International Conference on Coastal Engineering*, American Society of Civil Engineers, pp. 1983–1996.

JAGO, C.F. and HARDISTY, J., 1984. Sedimentology and morphodynamics of a macrotidal beach, Pendine Sands, SW Wales. *Marine Geology*, 60, 123–154.

LEE, G.H.; NICHOLLS, R.J., and BIRKEMEIER, W.A., 1998. Storm-driven variability of the beach-nearshore profile at Duck, North Carolina, USA, 1981–1991. *Marine Geology*, 148, 163–177.

LONGUET-HIGGINS, M.S., 1970. Longshore currents generated by obliquely incident sea waves. 1. *Journal of Geophysical Research*, 75, 6778–6789.

LONGUET-HIGGINS, M.S. and STEWART, R.W., 1964. Radiation stresses in water waves—a physical discussion with applications. *Deep-Sea Research*, 11, 529–562.

MASSELINK, G., 1993. Simulating the effects of tides on beach morphodynamics. *Journal of Coastal Research*, SI15, 180–197.

NIELSEN, P., 1984. Analytical determination of wave height. *Journal of Waterway, Port, Coastal and Ocean Engineering*, 110, 283–287.

OSBORNE, P.D. and GREENWOOD, B., 1992. Frequency dependent cross-shore suspended sediment transport. 2. A barred beach. *Marine Geology,* 106, 25–51

OSBORNE, P.D. and GREENWOOD, B., 1993. Sediment suspension under waves and currents: time scales and vertical structure. *Sedimentology*, 40, 599–622.

RIBBERINK, J.S. and AL-SALEM, A.A., 1995. Sheet flow and suspension of sand in oscillatory boundary layers. *Coastal Engineering*, 25, 205–225.

RUESSINK, B.G.; HOUWMAN, K.T., and HOEKSTRA, P., 1998. The systematic contribution of transporting mechanisms to the cross-shore

sediment transport in water depths of 3 to 9 m. *Marine Geology*, 152, 295–324.

RUSSELL, P.E. and HUNTLEY, D.A., 1999. A cross-shore "shape function" for high energy beaches. *Journal of Coastal Research*, 15, 198–205.

SALLENGER, A.H. and HOLMAN, R.A., 1985. Wave energy saturation on a natural beach of variable slope. *Journal of Geophysical Research*, 90, 11939–11944.

SHORT, A.D., 1991. Macro-meso tidal beach morphodynamics—an overview. *Journal of Coastal Research*, 7, 417–436.

SONU, C.J., 1972. Field observation of nearshore circulation and meandering currents. *Journal of Geophysical Research*, 77, 3232–3247.

SVENDSEN, I.A., 1984. Mass flux and undertow in a surf zone. *Coastal Engineering*, 8, 347–365.

THORNTON, E.B.; HUMISTON, R.T., and BIRKEMEIER, W., 1996. Bar/trough generation on a natural beach. *Journal of Geophysical Research*, 101, 12097–12110.

THORNTON, E.B. and GUZA, R.T., 1982. Energy saturation and phase speeds measured on a natural beach. *Journal of Geophysical Research*, 87, 9499–9508.

THORNTON, E.B. and GUZA, R.T., 1989a. Wind wave transformation. *In:* SEYMOUR, R.J. (ed) *Nearshore Sediment Transport*, Plenum Press, New York, pp. 137–171.

THORNTON, E.B. and GUZA, R.T.., 1989b. Nearshore circulation. A. Conservation equations for unsteady flow. *In:* SEYMOUR, R.J. (ed) *Nearshore Sediment Transport*, Plenum Press, New York, pp. 183–203.

THORNTON, E.B. and KIM, C.S., 1993. Longshore current and wave height modulation at tidal frequency inside the surf zone. *Journal of Geophysical Research*, 98, 16509–16519.

VAN RIJN, L.C., 1993. *Principles of Sediment Transport in Rivers, Estuaries and Coastal Seas.* Aqua Publications, Amsterdam.

WOLF, F.C.J., 1997. *Hydrodynamics, Sediment Transport and Daily Morphological Development of a Bar-Beach System.* Netherlands Geographical Studies, 232, Department of Geography, University of Utrecht, 267pp.

WRIGHT, L.D., 1976. Nearshore wave-power dissipation and the coastal energy regime of the Sydney-Jervis Bay region, New South Wales: a comparison. *Australian Journal of Marine and Freshwater Research*, 27, 633–640.

WRIGHT, L.D.; NIELSEN, P.; SHORT, A.D., and GREENE, M.O., 1982. Morphodynamics of a macrotidal beach. *Marine Geology*, 50, 97–128.

WRIGHT, L.D.; SHORT, A.D.; BOON, J.D.; KIMBALL, S., and LIST, J.H., 1987. The morphodynamic effects of incident wave groupiness and tide range on an energetic beach. *Marine Geology*, 74, 1–20.